Journal of Iberian Geology (2021) 47:483–500
https://doi.org/10.1007/s41513-020-00144-x

RESEARCH PAPER

The autopodial skeleton of *Paracamelus aguirrei* (Morales 1984) (Tylopoda, Mammalia) from the late Miocene site of Venta del Moro(Valencia, Spain)

Óscar Caballero[1] · Plini Montoya[1] · Vicente D. Crespo[2,3,4] · Jorge Morales[5] · Juan Abella[6,7]

Received: 3 March 2020 / Accepted: 27 October 2020 / Published online: 11 January 2021

Abstract
Venta del Moro is a classical locality from the late Miocene (Ventian, MN13) of the Cabriel basin from Valencia (Spain). This site is the type locality of nine mammal species. Among them, is the camelid *Paracamelus aguirrei*, which was defined by its upper dentition, a lower third premolar (p3), and some postcranial remains. This genus, which is the only Neogene camelid present in Europe, rapidly expanded throughout Eurasia from North America. In this work, the autopodial elements of *P. aguirrei* recovered from Venta del Moro are described, among them some that were previously unknown. This study shows that *P. aguirrei* was considerably large, comparable in size to the giant camels of North America like *Megacamelus merriami* and the giant camels of Eurasia like *Paracamelus gigas* and *Camelus knoblochi.*

Keywords Camelidae · Anatomy · Biometry · Neogene

Resumen
Venta del Moro es una localidad clásica del Mioceno final (Ventiense, MN13) de la cuenca del Cabriel de Valencia (España). Este yacimiento es la localidad tipo de nueve especies de mamíferos. Entre ellas se encuentra el camélido *Paracamelus aguirrei*, que fue descrito a partir de su dentición superior, un tercer premolar inferior (p3) y algunos elementos del esqueleto postcraneal. Este género, que es el único camélido presente en Europa durante el Neógeno, se expandió rápidamente a lo largo de toda Eurasia desde América del Norte. En este trabajo se describen los elementos autopodiales de *P. aguirrei* recuperados de Venta del Moro, algunos de ellos descritos por primera vez. Este estudio muestra que *P. aguirrei* fue un camélido de tamaño grande, similar en talla a las formas gigantes norteamericanas como *Megacamelus merriami* y a las formas gigantes euroasiáticas como *Paracamelus gigas* y *Camelus knoblochi*.

Palabras clave Camelidae · Anatomía · Biometría · Neógeno

Supplementary Information The online version contains supplementary material available at https://doi.org/10.1007/s41513-020-00144-x.

✉ Óscar Caballero
oscachor@alumni.uv.es

[1] Departament de Botànica i Geologia, Universitat de València, Doctor Moliner 50, 46100 Burjassot, Spain

[2] División de Paleontología de Vertebrados, Consejo Nacional de Investigaciones Científicas y Técnicas, Museo de La Plata (UNLP), La Plata, Argentina

[3] Museu Valencià d'Història Natural, P.O. Box 8460, L'Hort de Feliu, Alginet, 46018 Valencia, Spain

[4] Museo Paleontológico de Alpuente, Alpuente, Spain

[5] Museo Nacional de Ciencias Naturales (CSIC), Madrid, Spain

[6] Institut Català de Paleontologia Miquel Crusafont, Universitat Autònoma de Barcelona, Edifici ICTA-ICP, Carrer de les Columnes s/n, Campus de la UAB, Cerdanyola del Vallès, 08193 Barcelona, Spain

[7] Instituto Nacional de Biodiversidad, Pje. Rumipamba N. 341 y Av. de los Shyris (Parque La Carolina), Quito, Ecuador

1 Introduction

Venta del Moro is a classical late Miocene paleontological site from Valencia (Spain) (Fig. 1), widely known for its vertebrate faunal content, but also rich in invertebrate material and flora (Morales, 1984; Montoya et al. 2006; Casas-Gallego et al. 2015). According to recent magnetostratigraphical analyses, the estimated age of the site is 6.23 Ma (Gibert et al. 2013). It is known for being the reference locality of the Ventian mammal age (7–5 Ma), equivalent to the late Turolian (Morales et al. 2013). Venta del Moro is the type locality of nine species of mammals: the ursoid *Agriotherium roblesi* Morales & Aguirre, 1976, the camelid *Paracamelus aguirrei* Morales, 1984, the bovids *Tragoportax ventiensis* (Morales, 1984) and *Parabos soriae* Morales, 1984, the canid *Eucyon debonisi* Montoya et al. 2009, the mustelid *Martes ginsburgi* Montoya et al. 2011, the glirid *Eliomys yevesi* Mansino et al. 2015, and the bats *Pipistrellus rouresi* Crespo et al. 2018, and *Rhinolopus antonioi* Crespo et al. 2018. This site was first excavated from 1969 to 1980 by a team of the Museo Nacional de Ciencias Naturales (CSIC, Madrid) and studied by Aguirre et al. (1973), Morales and Aguirre (1976), and Morales (1984). Later, from 1995 to 2012 the site was excavated again by

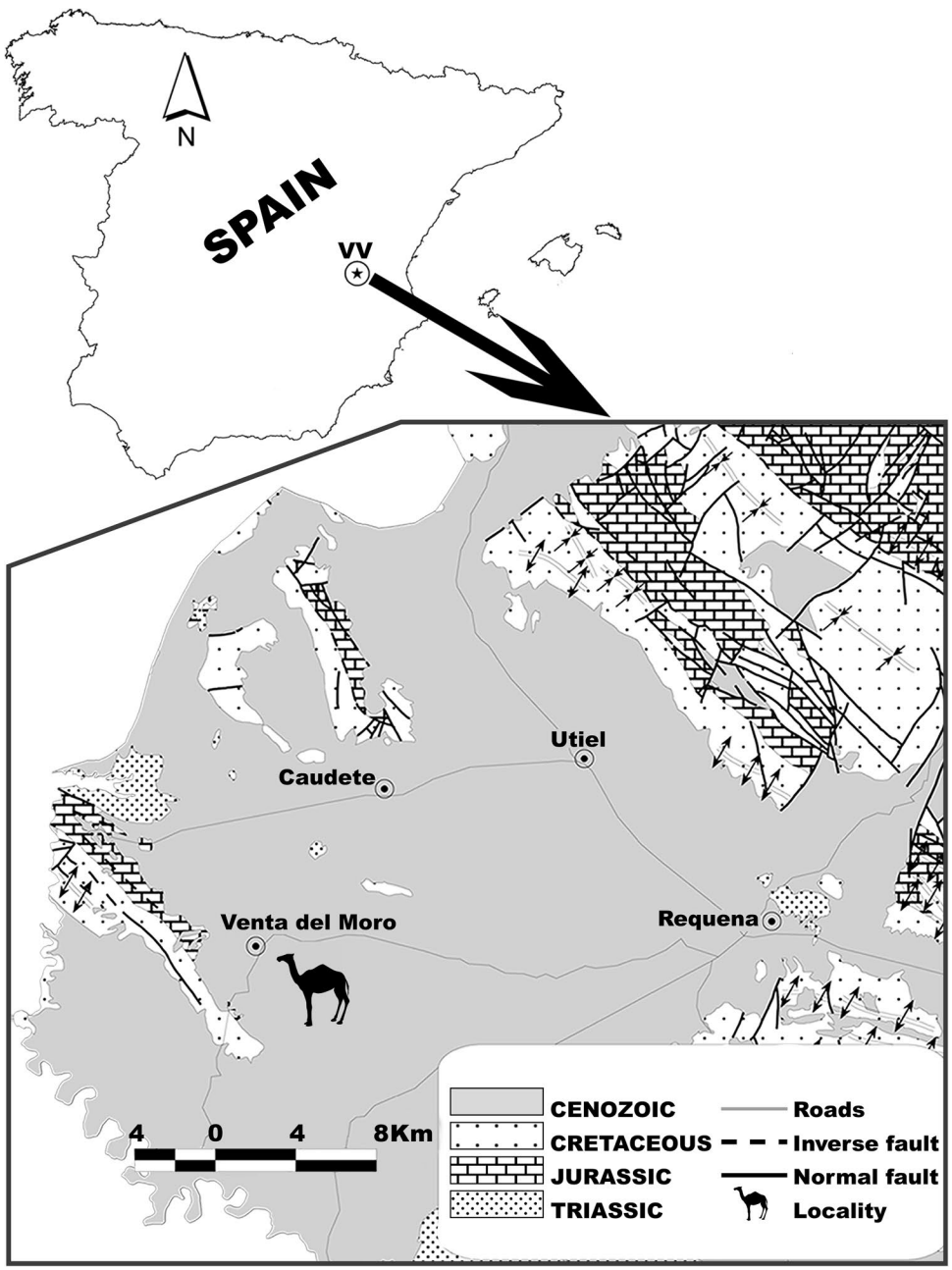

Fig. 1 Geological map from the area of Venta del Moro (Cabriel basin, Valencia, Spain) with the geographical situation of the palaeontological site (Modified from Mansino et al. 2014)

a team of the University of Valencia, although most of the material recovered is yet to be studied (Montoya et al. 2006; Morales et al. 2011). The site has more than 100 faunistic species in addition to vegetal remains and foraminifera (Morales et al. 2011). Pollen and faunal analyses suggest a savannah-mosaic paleoenvironment (Casas-Gallego et al. 2015). More detailed information on the faunal assemblage of Venta del Moro is found in Morales (1984), Montoya et al. (2006, 2009, 2011), Pesquero et al. (2007), Salesa et al.

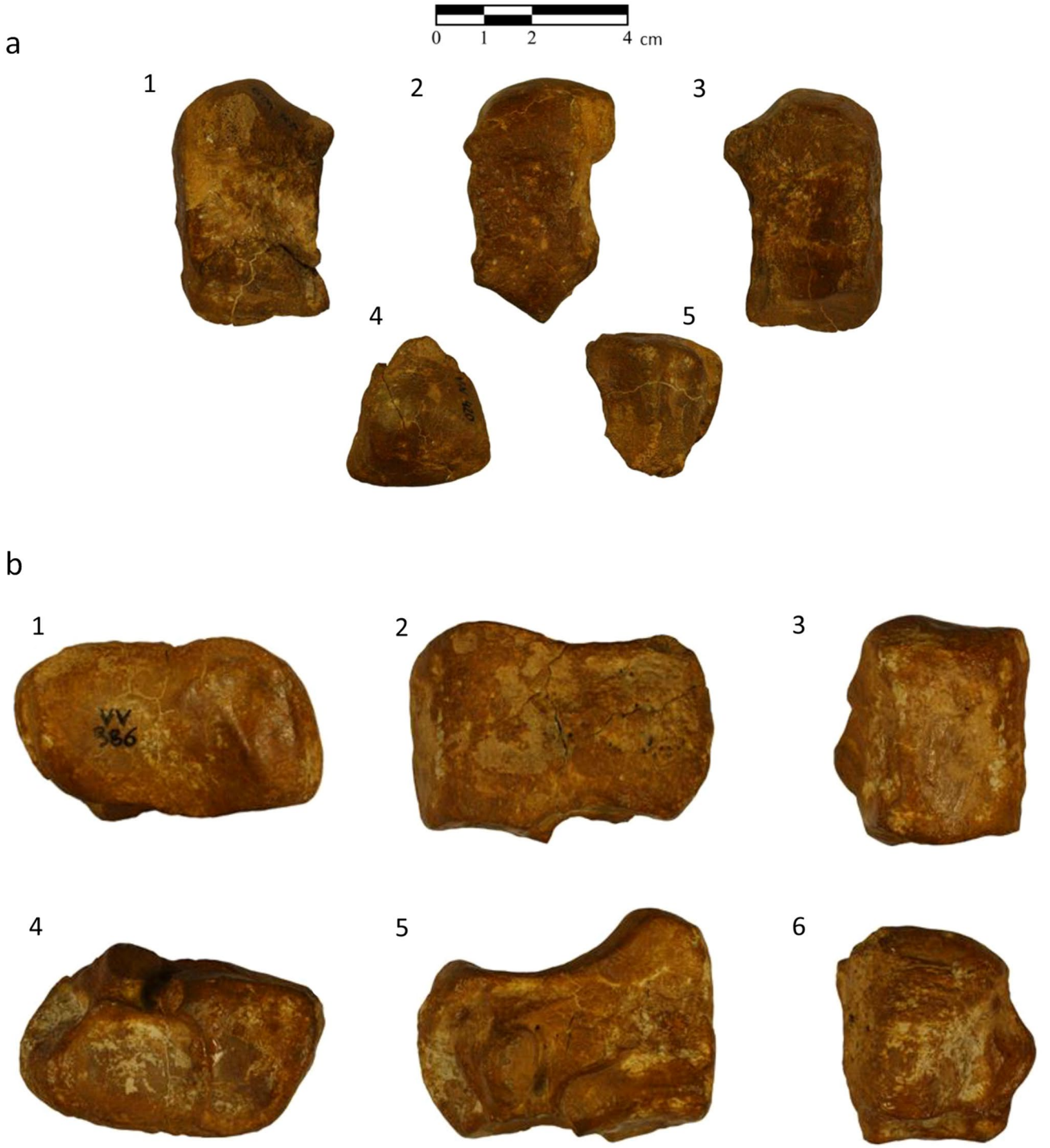

Fig. 2 *Paracamelus aguirrei* from Venta del Moro, Spain. **a** Lunate (VV-420) (1. Medial view, 2. Cranial view, 3. Lateral view, 4. Proximal view, 5. Distal view); **b** scaphoid (VV-386) (1. Proximal view, 2. Medial view, 3. Cranial view. 4. Distal view, 5. Lateral view, 6. Caudal view)

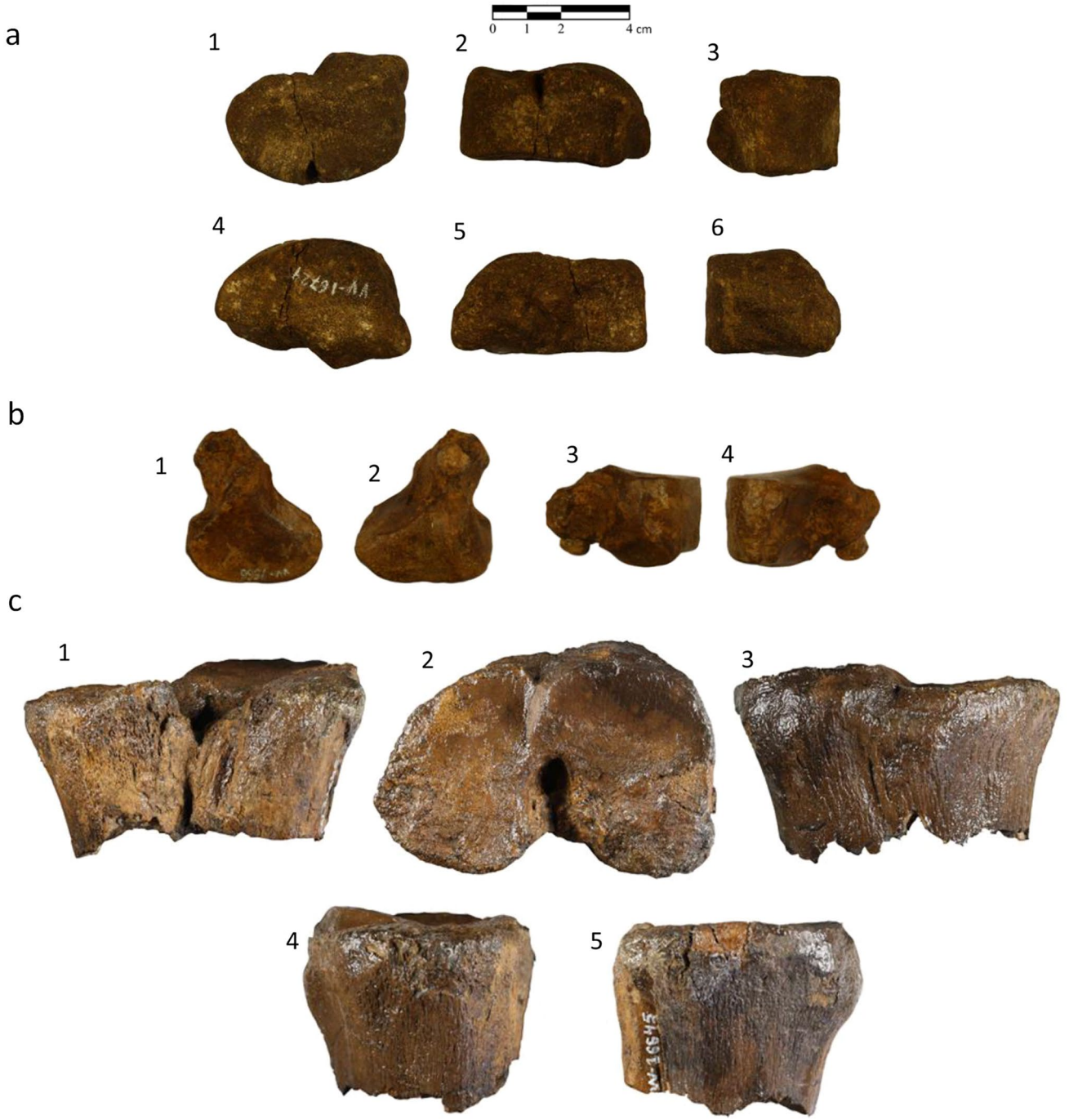

Fig. 3 *Paracamelus aguirrei* from Venta del Moro, Spain. **a** Hamate (VV-16,729) (1. Proximal view, 2. Lateral view, 3. Cranial view, 4. Distal view, 5. Medial view, 6. Caudal view); **b** capitate (VV-9566) (1. Proximal view, 2. Distal view, 3. Lateral view. 4. Medial view); **c** proximal metacarpal epiphysis (VV-16,645) (1. Caudal view, 2. Proximal view, 3. Cranial view, 4. Lateral view, 5. Medial view)

(2010), Mansino et al. (2014, 2015, 2017, 2018), Alba et al. (2015) and Crespo et al. (2018).

The Camelidae (order Artiodactyla, suborder Tylopoda) appeared in North America approximately 45 Ma, during the middle Eocene (Honey et al. 1998; Prothero and Schoch 2002). Camelids present some unique characteristics among artiodactyls, like the digitigrade state. Its particular walking pattern, known as *pace*, is effective for long-legged animals (Prothero and Schoch 2002). Camelid skulls differ from other hoofed mammals in the absence of cranial appendages, in having a completely fused mandibular symphysis, a tympanic bulla full of cancellous bone, I3 caniniform in most of the

Fig. 4 *Paracamelus aguirrei* from Venta del Moro, Spain. Metacarpal (VV-14,946) (1. Cranial view, 2. Caudal view)

cases, spatula-like lower incisors, both p1 and P1 absent or caniniform, and upper molars with four cuspids each. The postcranial skeleton of camelids is distinguished for an elongated neck, radius and ulna coosified, very reduced fibula, not fused navicular and cuboid, nor trapezoid and capitate, completely fused metapodials III-IV except at the divergent distal epiphysis in derived forms and completely unfused in the basal genera (for the complete listing see Honey et al. 1998).

The family Camelidae spread to the Old World during the late Miocene or pre-Messinian (Pickford et al. 1993) and to South America during the end of the Pliocene (Labarca et al. 2013, and references therein). *Paracamelus* Schlosser 1903 is the only extinct camelid genus known in the Old World during the Mio-Pliocene (Schlosser 1903; Zdansky 1926; Pickford et al. 1995). This genus was considered exclusive from Europe, Asia, and Africa until the discovery of the Yukon camel remains (considered as cf. *Paracamelus gigas* (Harrington 2011)) from the Plio-Pleistocene of the Yukon area (Canada) and the remains from Ellesmere Island (Canada) (Rybczynski et al. 2013). The American ancestor of *Paracamelus* is still unknown, although the most probable genera are *Megatylopus* (Honey et al. 1998, and references therein), *Procamelus*, *Megacamelus*, and *Titanotylopus* (Pickford et al. 1995). Supposedly *Paracamelus* migrated to the Old World from North America through the Beringian land bridge during MN12 (7.9–7.0 Ma) (Titov and Logvynenko 2006; Morales et al. 2013) and rapidly spread across Eurasia and probably Africa (Pickford et al. 1995), reaching the Iberian Peninsula before the Messinian Salinity Crisis which affected the Mediterranean between 5.97 and 5.33 million years ago (Pickford et al. 1993; 1995; Gibert et al. 2013; García-Alix et al. 2016). Besides *P. aguirrei*, more *Paracamelus* species appeared during the expansion of the genus: *P. gigas* Schloser, 1903 (late Pliocene of China), *P. alutensis* (Stefanescu, 1895) (Plio-Pleistocene of Eastern Europe), and *P. alexejevi* Khavesson, 1959 (early Pliocene of Ukraine) (Titov and Logvynenko 2006, and references therein). Although the evolutionary relationships between different species of *Paracamelus* are unclear, some authors suggest that *P. alexejevi* was a descendent of *P. aguirrei* (Made and Morales 1999). *Paracamelus aguirrei* could have arrived in the Iberian Peninsula through two different routes: the African route, crossing from Asia to Africa and later to the Iberian Peninsula across today's current Strait of Gibraltar (Pickford et al. 1993; 1995; Agustí et al. 2006; Gibert et al. 2013); and the European route, crossing from Asia throughout Europe towards the Iberian Peninsula (Titov and Logvynenko 2006). *Paracamelus aguirrei* is the oldest and the most occidental taxon of the Eurasian camelid fossil record (Morales et al. 1980; Pickford et al. 1993; Titov and Logvynenko 2006; Gibert et al. 2013).

Besides the remains from Venta del Moro, in the Iberian Peninsula, *Paracamelus* is also known from the site of Librilla (Alberdi et al. 1981; Pickford et al. 1995). The ichnites of *Paracamelichnum* from Hoya de la Sima (Jumilla; Pérez-Lorente et al. 2009) are attributed to *Paracamelus*. Both sites are in the Region of Murcia and are contemporaneous with Venta del Moro.

Here we describe the new remains of the autopodial skeleton of *P. aguirrei* from Venta del Moro (Valencia). Within these new remains, seven new anatomical elements of the autopodium are described here for the first time (the lunate, the scaphoid, the hamate, the capitate, the metacarpal II-IV, the malleolar, and the intermediolateral cuneiform). Furthermore, complete descriptions for the only five autopodial elements that had previously been published (the calcaneus, the astragalus, the cuboid, the navicular, and the phalanges) have been performed.

2 Materials and methods

2.1 Abbreviations and measurements

Measurements were taken to the nearest 0.1 mm using a Mitutoyo caliper (Supplementary files I).


a
1
2
3
4
5
6
0 1 2 4 cm
b
1
2
3
4
5
6

◂**Fig. 5** *Paracamelus aguirrei* from Venta del Moro, Spain. **a** Astragalus (VV-17,334) (1. Medial view, 2. Caudal view, 3. Proximal view, 4. Lateral view, 5. Cranial view, 6. Distal view); **b** Calcaneus (VV-6795) (1. Medial view, 2. Lateral view, 3. Cranial view. 4. Caudal view, 5. Proximal view, 6. Distal view)

For the autopodium, the measurements of Martini et al. (2018) were followed.

The abbreviations used in this text are the following:

MN: Mammal Neogene Zones of Mein (1975).

MUVHN: Museu de la Universitat de València d'Història Natural, Valencia, Spain.

MNCN: Museo Nacional de Ciencias Naturales-CSIC, Madrid, Spain.

VV: Venta del Moro, Valencia.

2.2 Studied material

The newly described fossil remains of *Paracamelus aguirrei* are stored at the MUVHN. They consist of the following:

One lunate (VV-420 (right)), two capitates (VV-9566 (left) and VV-3456 (left)), one navicular (VV-9156 (right)), 6 first phalanges (VV-10,233, VV-10,708, VV-16,097, VV-1890, VV-16,068 and VV-7419), three astragali (VV-17,334 (right), VV-7580 (left) and VV-16,202 (right)), two calcani (VV-6975 (left) and VV-7070 (left)), two cuboids (VV-17,335 (left) and VV-6976 (right)), four malleoli (VV-14,006 (right), VV-7494 (left), VV-7620 (left) and VV-3893 (left)), one intermediolateral cuneiform (VV-10,691 (right)), one hamate (VV-16,729 (left)), one scaphoid (VV-386 (right)), two metacarpal proximal epiphysis (VV-1853 (left) and VV-16,645 (left)) and one metacarpal without distal epiphysis (VV-14,946 (left)).

2.3 Comparative taxa

For the anatomical and biometrical comparison to other camelid taxa the following bibliographic materials were used:

Camelops hesternus Leidy, 1873 (Webb 1965; Zazula et al. 2016) from the Pleistocene of Rancho la Brea (California) and the Pleistocene of Alaska and Yukon (Canada), the extant *Camelus bactrianus* Linnaeus, 1758 (Martini et al. 2018) from Asia (Ji et al. 2009, and references therein; Mukasa-Mugerwa 1981, and references therein), *Camelus dromedarius* Linnaeus, 1758 (Martini et al. 2018) from Asia, and Africa (Mukasa-Mugerwa 1981, and references therein), and *Camelus bactrianus ferus* (Titov and Logvynenko 2006, and references therein) from the deserts of China and Mongolia (Ji et al. 2009, and references therein), *Camelus knoblochi* Nehring, 1901 (Havesson 1954 in Titov 2008) from the Middle Pleistocene of Volga River Region (Russia), *Camelus thomasi* Pomel, 1893 (Martini & Geraads 2018) from the Middle Pleistocene of Thigennif (Algeria), *Gigantocamelus fricki* Barbour & Schultz 1939 (Barbour and Schultz 1939) from the Lower Pleistocene of Lisco quarries (Nebraska), *Megacamelus merriami* Frick, 1921 (Harrison 1985) from the latest Miocene-Early Pliocene of Keams Canyon (Arizona), *Paracamelus* cf. *aguirrei* (Titov and Logvynenko 2006) from the late Miocene of Novocherkassk (Russia), *Paracamelus alexejevi* (Havesson 1954; Morales 1984; Havesson 1954; Logvinenko 2000; Titov and Logvynenko 2006) from the early Pliocene of Kuchurgan and Odessa (Ukraine), *Paracamelus alutensis* (Titov & Logvynenko 2006) from the late Pliocene of Khapry (Russia), *Paracamelus gigas* (Zdansky 1926 in Morales 1984; Zdansky 1926, and Teilhard and Trassaert 1937 in Titov & Logvynenko 2006) from the late Pliocene of China, *Paracamelus praebactrianus* (Orlov, 1927) (Orlov 1929, and Havesson 1954 in Titov and Logvynenko 2006) from the middle-late Pliocene of Kazakhstan, and *Titanotylopus* Barbour & Schultz, 1934 (Harrison 1979) from the late Miocene to the Pleistocene of North America.

3 Systematic paleontology

Order: Artiodactyla Owen, 1848.

Suborder: Tylopoda Illiger, 1811.

Family: Camelidae Gray, 1821.

Subfamily: Camelinae Gray, 1821.

Tribe: Camelini Gray, 1821.

Genus: *Paracamelus* Schlosser, 1903.

Type species: *Paracamelus gigas* Schlosser, 1903.

Type localities: Honan and Tiensin, China.

Age: late Pliocene (4.9–0.8 Ma) (Wang et al. 2013).

Diagnosis: After Likius et al. 2003:

Paracamelus species larger than the extant *C. bactrianus* and *C. dromedarius* and characterized by the presence of p3, elongated metapodials with distinctive metacarpal proximal articular facets (subquadrangular in Mc IV and subtriangular in Mc III) and deep plantar gutters under the proximal epiphysis of the metatarsal.

Other Species: *Paracamelus alexejevi* Khavesson, 1954, *Paracamelus aguirrei* Morales, 1984, *Paracamelus alutensis* (Stefanescu, 1895), *Paracamelus kuljenensis* Khomenko, 1915, *Paracamelus praebactrianus* (Orlov, 1927).

Paracamelus aguirrei Morales, 1984.

1980 *Paracamelus* nov. sp. Morales, Soria & Aguirre, p. 139.

1993 *Paracamelus*; Pickford et al., p. 701.

1995 *Paracamelus*; Pickford et al., p. 642.

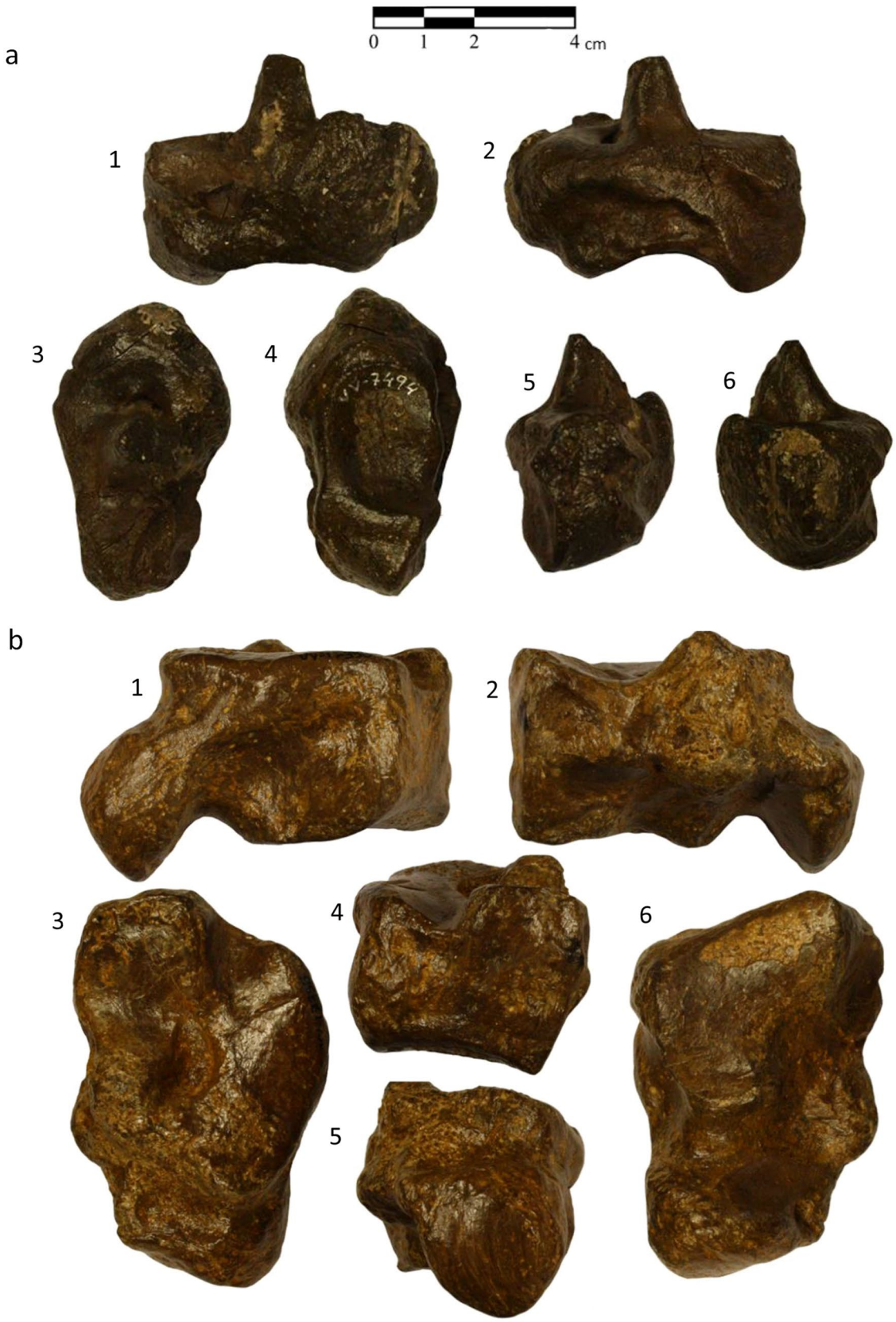
0 1 2 4 cm
a
1
2
3
4
JV-7494
5
6
b
1
2
3
4
5
6

◂**Fig. 6** *Paracamelus aguirrei* from Venta del Moro, Spain. **a** Malleolar (VV-7494) (1. Lateral view, 2. Medial view, 3. Proximal view, 4. Distal view, 5. Cranial view, 6. Caudal view); **b** Cuboid (VV-17,335) (1. Lateral view, 2. Medial view, 3. Proximal view. 4. Cranial view, 5. Caudal view, 6. Distal view)

1999 *Paracamelus aguirrei* Made & Morales, 1994, p. 221.
1999 *Paracamelus aguirrei* Kostopoulos & Sen, p. 189.
2001 *Paracamelus aguirrei* Logvynenko, p. 41.
2002 *Paracamelus aguirrei* Made et al. p. 329.
2003 *Paracamelus aguirrei* Likius et al. p. 189.
2006 *Paracamelus* cf. *aguirrei* Titov & Logvynenko, p. 163.
2006 *Paracamelus aguirrei* Titov & Logvynenko, p. 163.
2006 *Paracamelus aguirrei* Made et al. p. 235.
2006 *Paracamelus aguirrei* Montoya et al. p. 314.
2013 *Paracamelus*; Rybczynski et al. p-2.
2013 *Paracamelus aguirrei* Gibert et al. p. 691.
2013 *Paracamelus aguirrei* Morales et al. p. 152.
2017 *Paracamelus aguirrei* Colombero et al. p. 515.

Diagnosis: In Morales (1984), translated from Spanish. *Paracamelus* of intermediate size between *P. alexejevi* and *P. gigas*. Dentition with small M3 and large M1 in relation to the molar series (M1-M3). Robust M2. The p3 is reduced as it occurs with the other species of the genus. Postcranial skeleton morphologically different from *P. gigas* and *P. alexejevi*. Phalanx I notably bigger and more robust than *P. alexejevi* and similar to *P. gigas*.

Type locality: Venta del Moro, Valencia, Spain.

Age: late Miocene, 6.23 Ma.

Other localities: *Paracamelus* cf. *aguirrei*, Pontian deposits, Odessa, Ukraine (Titov and Logvynenko 2006).

3.1 Descriptions

Lunate (Fig. 2a): The only preserved lunate lacks the entire caudal body, only the cranial part is preserved. It is a complex structure due to its multiple articulation facets for the rest of the carpal bones. The proximal portion is dome-shaped. In medial view, four facets belong to the radius, the scaphoid (two) and the capitate. The facet for the radius is located at the proximal part and is rectangular-shaped, distally there are the facets for the scaphoid, which are subtriangular-shaped and are separated by a groove, finally at the most distal part is the facet for the capitate, which has a rectangular shape. In lateral view, four facets belong, proximally to distally, to the radius, the pyramidal (two), and the hamate. The facet for the radius and the proximal facet for the pyramidal are very damaged and no clear shape is observed, the distal facet for the pyramidal and the facet for the hamate are rectangular-shaped.

Scaphoid (Fig. 2b): The scaphoid of *P. aguirrei* is rectangular. It is slightly more elongated in the horizontal axis when compared to *C. dromedarius*, and in distal view, the cranial side of *P. aguirrei* looks more triangular than in *C. dromedarius*. The proximal view is entirely occupied by the facet for the radius. The distal view is formed by the facets of the capitate, the trapezoid, and the lunate. The capitate facet is situated at the cranial side of the view and is triangular-shaped, next to it is the trapezoid facet, which is concave and elongated in the horizontal axis, and finally, the lunate facet is situated in the caudolateral part and is elliptic. In lateral view, the rest of the lunate facets are found, one in the caudal side and two on the cranial side. The most caudal one protrudes laterally, is oval-shaped, and is also seen from the distal view. The other two facets are placed in the cranial zone; one being triangular and situated in the proximal side, while the other is elliptical and placed in the distal side.

Hamate (Fig. 3a): Slightly sub-elliptical shape. The hamate seems to be curvier in general and the caudal projection looks bigger in *C. dromedarius* than in *P. aguirrei*. However, these differences may be due to the state of the fossils. In cranial view, the pyramidal facet can be seen occupying most of the surface except for the craniomedial part, where the lunate facet is located. The pyramidal facet is elliptical following the sigmoidal form of that part of the bone, while the lunate facet is triangular-shaped and separated from the other facet by an elevation. In medial view, two prominent peaks are found near the capitate facets. At least two capitate facets can be observed, although due to the conservation of the fossil we cannot discard that it could originally have more. The most cranial one is rectangular in the proximodistal axis, while the second is elliptical and is situated in one of the bone projections. The distal view is entirely occupied by the metacarpal facet, which has an arrow-like shape.

Capitate (Fig. 3b): Proximodistally flattened bone. In the capitate of *P. aguirrei*, the caudal side seems to be more elongated and thinner than in *C. dromedarius*. The capitate is formed by a subtriangular body with a protuberance in the caudal part. The facets for the scaphoid and the lunate are located in the main body, the former being larger than the latter. The scaphoid facet is triangular and slightly concave while the lunate facet is rectangular and inclined laterally, where the two hamate facets are found. The first facet of the hamate is rectangular in the proximodistal axis and is situated next to the lunate one, while the second one is located in the caudal protuberance and it is triangular. In medial view, at least two trapezoidal facets can be seen. The most proximal one is elliptical and limits with the facet for the scaphoid, while the most distal one is circular and limits with the facet for the metacarpal. In distal view, the metacarpal facet occupies all the subtriangular body. In the caudal protuberance, only the facet for the hamate is observed.

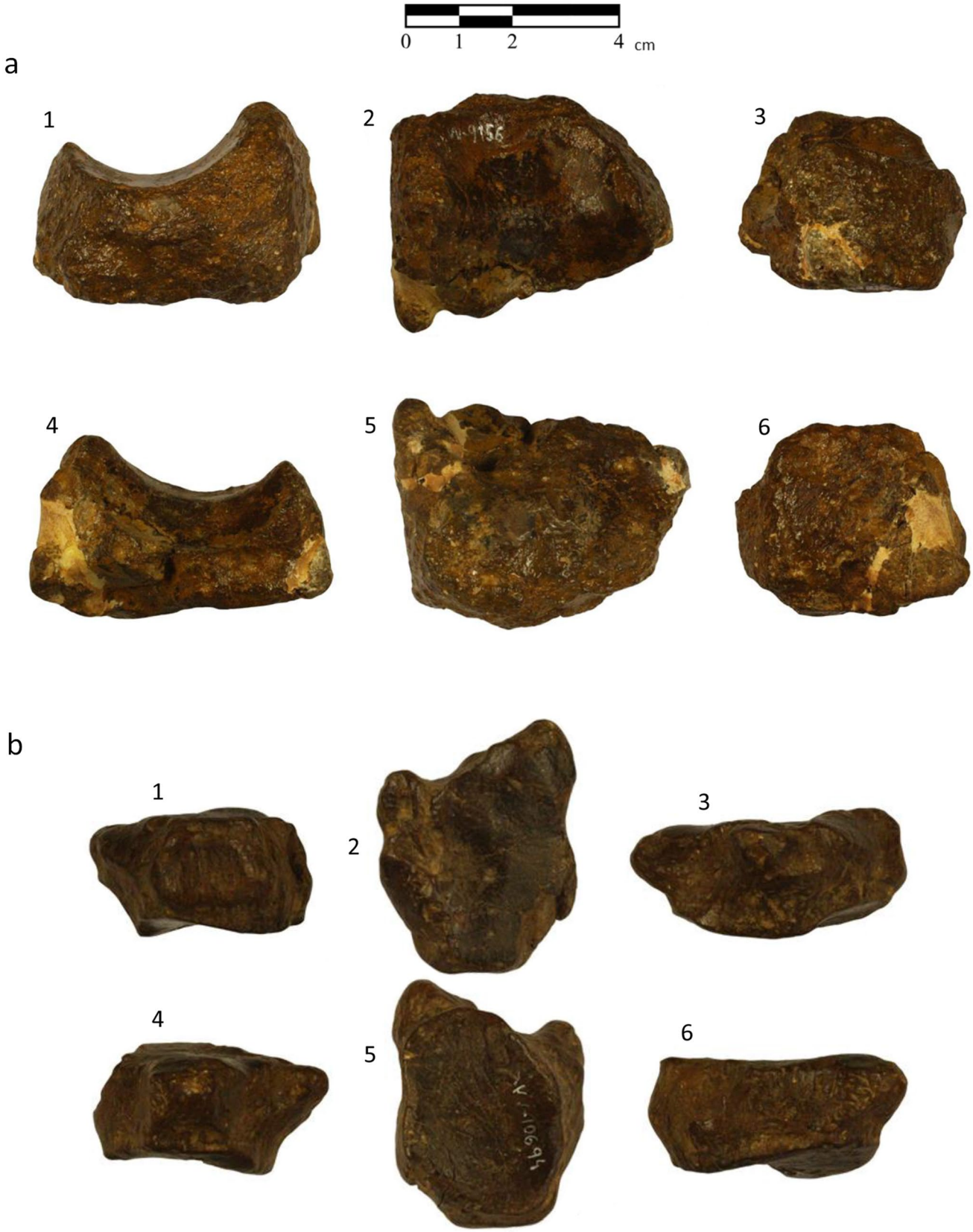
0 1 2 4 cm
a
1
2
3
4
5
6
b
1
2
3
4
5
6

◂**Fig. 7** *Paracamelus aguirrei* from Venta del Moro, Spain. **a** Navicular (VV-9156) (1. Medial view, 2. Proximal view, 3. Cranial view, 4. Distal view, 5. Lateral view, 6. Caudal view); **b** intermediolateral cuneiform (VV-10,694) (1. Cranial view, 2. Proximal view, 3. Lateral view. 4. Caudal view, 5. Distal view, 6. Medial view)

Metacarpal II-IV (Figs. 3c and 4): In the specimen, the distal epiphysis has not been preserved. The proximal epiphysis is horseshoe-shaped and has three facets. The hamate facet is the biggest one occupying half of the proximal side, followed by the facet for the capitate and by the facet for the trapezoid. The hamate facet is the most lateral and is teardrop-shaped, the capitate facet limits laterally with the hamate facet and caudally with the trapezoid facet and has a sub-elliptical form, and finally, the trapezoid facet is the most caudal one and is subtriangular-shaped. Between the three facets, there is a kidney-like pit. The proximal epiphysis is surrounded by a rugose surface for the attachment of the tendon for the extensor carpi radialis muscle, which is wider in its medial side. The diaphysis is convex in the caudal side and straight in the cranial one. The palmar longitudinal groove is U-shaped.

Astragalus (Fig. 5a): Rectangular in shape. The studied astragali have a less marked fibular salient compared to the one present in *Cp. hesternus*, *C. thomasi*, and *C. bactrianus*. In proximal view, there are two crests whereas in the distal one there are two condyles. The lateral crest is higher than the medial one. The caudal view is dominated by the plantar trochlea (also known as sustentacular facet), which is convex and rectangular shaped. The subsustentacular fossa is placed in the distal part of the plantar trochlea and slightly fuses laterally. The subsustentacular fossa of the specimen VV-17,334 is divided into two by a partition wall. In cranial view, there is the astragalus sinus, which is concave and follows the form of the plantar trochlea. In lateral view, there are three facets which are, proximally to distally, the fibular facet, the parasustentacular facet, and the paracuboid facet. The fibular facet is curved and follows the form of the lateral crest. The parasustentacular facet is inversely placed to the fibular facet and follows the shape of the plantar trochlea. Finally, the paracuboid facet is subelliptically-shaped and is situated in the most distal part, limiting with the lateral trochlea. The fibular facet ends distally in the fibular salient. The paracuboid facet is separated from the fibular salient by a fossa. In medial view, in the distal part, there is the navicular facet, which is curved following the form of the medial trochlea and continues in the distal view of the medial trochlea. In the proximal end of the navicular facet, there is a fossa. Another smooth surface is found in the medial part of the medial crest. The tibial ligament surface is oblique and connects the plantar trochlea with the medial side. Finally, the distal view coincides with the continuation of the navicular facet and the cuboid facet. The navicular facet is hourglass-shaped and occupies all the medial distal condyle and the medial part of the lateral condyle, while the cuboid facet is rectangular in the craniocaudal axis and only occupies the lateral part of the lateral condyle.

Calcaneus (Fig. 5b): The calcaneus of *P. aguirrei* is more elongated and rectangular-shaped than those from *C. dromedarius*. The *tuber calcanei* of *P. aguirrei* is more elongated and less massive than *Cp. hesternus.* At the proximal end of the *tuber calcanei* there is a sub-pyramidal facet, which slightly remembers a pentagon when seen in proximal view. The articular facets and the *sustentaculum astragali* occupy the distal portion of the element. The *sustentaculum astragali* is elongated in the transversal axis more than in the sagittal axis. In the *sustentaculum astragali* there are the sustentacular facets, the first one occupies all the distal part of the *sustentaculum* and is slightly square-shaped with rounded edges, while the second one is situated on the cranial border of the *sustentaculum*, is small and subelliptically shaped. In medial view and distally from the *sustentaculum astragali* there is the distal astragular surface, which is concave, slightly elliptical, and elongated to the distal side. The cuboid facet is found in the most caudal zone, is large, and slightly rectangular in the proximodistal axis. The parasustentacular facet protrudes from the main body and connects with the fibular facet in the cranial part. The parasustentacular facet slightly resembles an inverted teardrop in medial view, is sigmoidal in its medial and lateral parts, and rounded in cranial view.

Malleolar (Fig. 6a): Small bone with a pyramidal central part. Distally, the calcaneum facet has an oval shape, which is slightly wider in the cranial part. In the proximal view, there is a protuberance that connects with the fibular incisura from the tibia.

Cuboid (Fig. 6b): It has a main rectangular body and a caudal protuberance, which curves ventrally. In the proximal view, the facet for the calcaneus occupies the major part of the main rectangular body, while the astragalus facet occupies the most craniomedial part. The calcaneus facet is slightly elliptical, although curved at the caudal end, and slightly concave. The astragalus facet is oval, concave, and creates a fossa, which ends cranially and caudally into an elevation. There is a little arista that separates the astragalus facet in two. Between both facets, there is a kidney-like pit that separates them. In distal view, the metatarsal facet occupies the whole main body and has an "L" shape, and in the caudal protuberance, there is a little oval facet for the metatarsal which is situated in the medial part of the protuberance. In medial view, the facets for the navicular occupy the proximal part, while the facets of the cuneiform are placed in the distal part, and there is a thin protuberant line, which separates both parts. There are at least three navicular facets and two cuneiform facets. The two first facets for the


0 1 2 4 cm
a
b
1
2
1
2
3
4
3
4
5
6
5
6

◂**Fig. 8** *Paracamelus aguirrei* from Venta del Moro, Spain. Proximal phalanges: **a** right phalanx (VV-16,047) (1. Cranial view, 2. Caudal view, 3. Medial view, 4. Lateral view, 5. Proximal view, 6. Distal view); **b** left phalanx (VV-16,048) (1. Caudal view, 2. Cranial view, 3. Lateral view. 4. Medial view, 5. Distal view, 6. Proximal view)

navicular occupy the cranioproximal part of the medial view, have a triangular shape, and are separated by a thin groove. The third navicular facet is located onto a peak that protrudes from the caudal part of the main body and is circular in shape. The first cuneiform facet occupies the craniodistal part of the medial view and is elliptical, while the second one is found distally from the protruded peak and is circular. In the original description of the cuboid, the fossa which separates the three facets of the cranial view is almost closed (Morales 1984), while in the new collection one of the cuboids has a completely open fossa (VV-6976) and the other one has it completely closed (VV-17,335) which indicates interspecific variability. In comparison with *C. thomasi* the caudal projection seems to be higher in the cuboids of *P. aguirrei*. In general, the new cuboids are similar to those of *C. bactrianus*.

Navicular (Fig. 7a): This specimen has a generally pyramidal shape. The only specimen of the sample is distally and medially broken and worn down. The two facets of the astragalus occupy the major part of the proximal view and are separated by a thin elevation. The lateral astragalus facet is the smaller of the two and is slightly crescent-shaped, while the medial astragalus facet is bigger and more rectangular. Both astragalus facets are concave. In the distal view the facet for the intermediolateral cuneiform, which is located in the cranial part, seems to be slightly elliptical, while the facet for the medial cuneiform occupies the caudal part and is more circular, but both facets are barely observable. Due to bone preservation, no other facets can be seen.

Intermediolateral cuneiform (Fig. 7b): Flattened bone in the proximodistal axis with semielliptical shape. *Paracamelus aguirrei* seems to have a sharper intermediolateral cuneiform than *C. bactrianus*. In cranial view, the navicular facet is kidney-shaped and is situated on the medial side, occupying most of the body. In distal view, the metatarsal facet has an ellipsoidal shape and fills the whole view. In medial view, there are two facets for the cuboid and a peak, which is found in the caudal part of the medial view and protrudes medially. The first cuboid facet is located in the cranial part of the medial view, has an elliptical shape, and limits with the caudal peak, occupying most of the medial view. The second cuboid facet is located onto the caudal peak and is tiny and oval. In the caudal view, there is a protuberance, which protrudes caudally and has a little contact zone, probably for the other cuneiform.

Phalanx I (Fig. 8): Typical camelid first phalanx with an hourglass shape. Both epiphyses are thicker than the diaphysis. The proximal epiphysis is horizontally flat and larger than the distal trochlea. The metapodial facet occupies all the proximal view of the proximal epiphysis. The rugose attachment area for the major suspensory ligament is located at the caudal part of the diaphysis, limiting proximally with the proximal epiphysis, and has an inverse V shape, which elongates to the distal part. In the distal condyles, there is a pit both medially and laterally. The anterior and posterior phalanges cannot be differentiated by its morphology or its size, in part due to the lack of comparative material of *Paracamelus*. The phalanges of *P. aguirrei* rugose attachment area for the major suspensory ligament show and intermediate state between *Titanotylopus* and *Camelus* (Harrison 1979), as *P. aguirrei* shows a shorter area than *Titanotylopus* and a larger area than *Camelus* (Harrison 1979).

4 Results

The size of the carpal and tarsal bones shows a wide range of variability, which may reflect marked sexual dimorphism affecting body size. In general, the smallest individuals of *P. aguirrei* are within the range of variability of the extant *Camelus* (Martini et al. 2018). But the largest individuals exceed by far the maximum values of the extant species. Hence, the females of *Paracamelus aguirrei* would have the height of the males of the extant species, but the male individuals would widely exceed the maximum values of size of the latter, approaching the giant species of the family (Figs. 9 and 10).

Both the lunate (Fig. 9a) and the scaphoid (Fig. 9b) show a big differentiation with the extant *Camelus* (Martini et al. 2018). The lunate of *P. aguirrei* is quite larger, approximately 16% larger in its maximum height, in cranial view, when compared to the one of the extant genus.

The scaphoid (Fig. 9b) is larger in *P. aguirrei* when compared to *C. dromedarius* (Martini et al. 2018) and *Cp. hesternus* (Webb 1965), around a 14% bigger in its maximum height, although there is not much difference with *C. bactrianus* (Martini et al. 2018), roughly a 3% larger in its maximum height.

The hamate (Fig. 9c) of *P. aguirrei* has an average size compared to that of the extant *Camelus* (Martini et al. 2018) and is placed exactly in a middle position within the measurements of the extant camels.

Similar to what occurs with the hamate (Fig. 9c), the capitate (Fig. 9d) of *P. aguirrei* is comparable in size with those from the living species of *Camelus* (Martini et al. 2018) and the extinct *Cp. hesternus* (Webb 1965).

Two plots show the biometrical results for the metacarpal, one with the measurements of the proximal epiphysis (Fig. 9e) and the other comparing the width of the proximal epiphysis with the dorsoventral length from the proximal

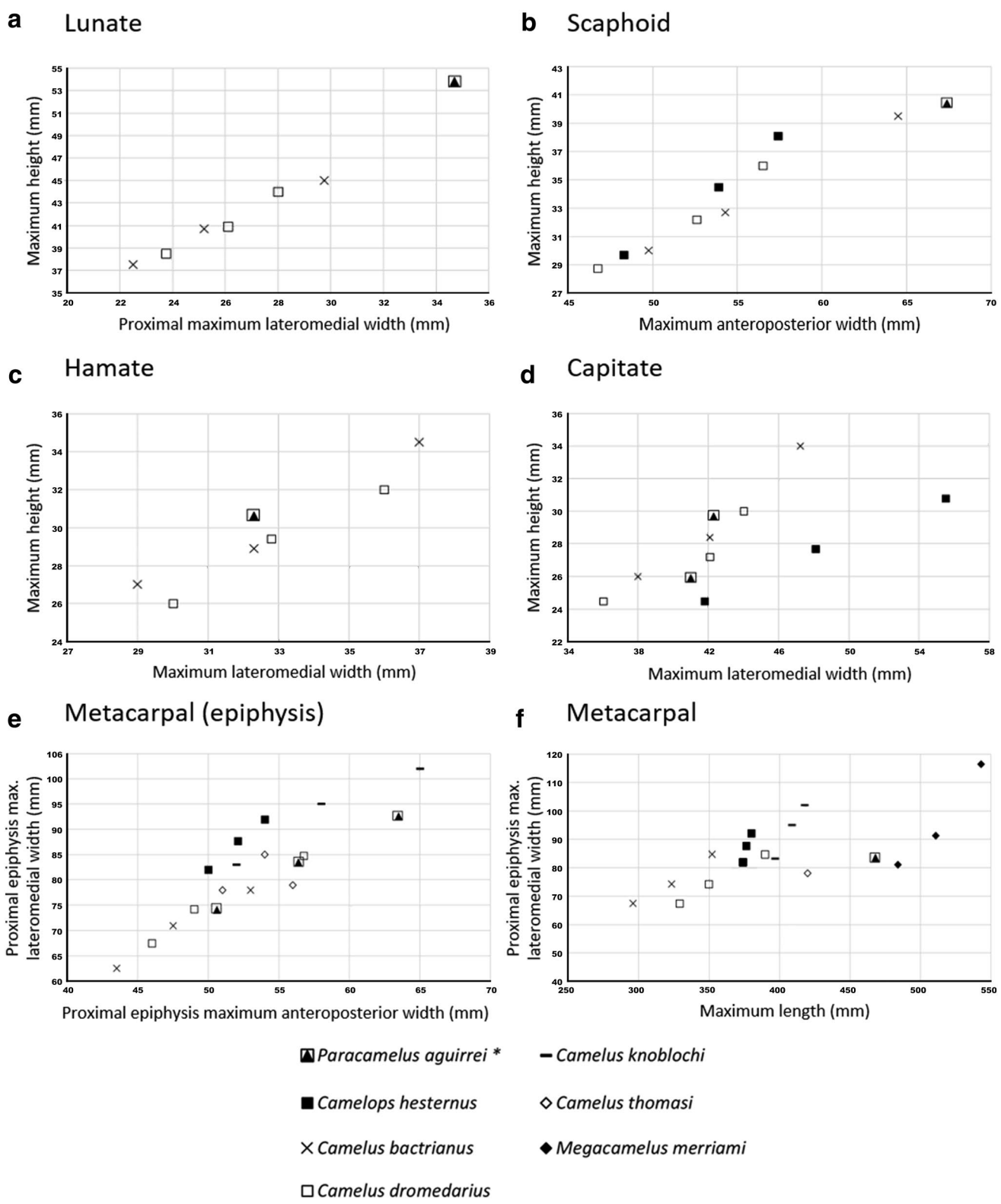

Fig. 9 Bivariate plots of the lunate (**a**); scaphoid (**b**), hamate (**c**), capitate (**d**), metacarpal proximal epiphysis (**e**) and metacarpal (**f**). The measurement of *Paracamelus aguirrei* is the length from the proximal epiphysis to the start of the distal epiphysis. In contrast the other specimens considered are complete metacarpals

epiphysis to the starting of the distal epiphysis in *P. aguirrei* and the ending of the distal epiphysis in the other species (Fig. 9f). This measurement has been used because the only *P. aguirrei* metacarpal that is preserved lacks the distal condyles. In the proximal epiphysis plot (Fig. 9e), there are three *P. aguirrei* specimens distributed all along with the biometrical space, going from the size of an average *C. dromedarius* (Martini et al. 2018) to the larger specimens of *C. knoblochi* (Titov 2008, and references therein), following the same spatial trend than the other taxa. On the other hand, in Fig. 9f the length of the metacarpal of *P. aguirrei*, corresponds to the largest values of the sample, reaching the minimum size of *M. merriami* (Harrison 1985) and being clearly larger than all the other extant and extinct species. *Paracamelus aguirrei* metacarpals are approximately 16% longer than extant *Camelus* (Martini et al. 2018) and the extinct *Cp. hesternus* (Webb 1965), and an 8% longer than *C. knoblochi* and *C. thomasi* (Martini and Geraads 2018). About this last comparison (Fig. 9f) it must be re-emphasized that the metacarpal of *P. aguirrei* lacks its distal condyles, which means that its maximum length is even larger. Also, in Fig. 9f the metacarpal of *P. aguirrei* is larger than those from the extant *Camelus* species and *Cp. hesternus* with similar proximal epiphysis width. This difference in the proportion of the metacarpal of *P. aguirrei* makes it more similar in its morphology to *M. merriami*, and *C. thomasi*, which also tend to have a longer metacarpal in relation to the width of the proximal epiphysis, while the extant *Camelus*, *C. knoblochi* and *Cp. hesternus* have a more square-like morphology.

The astragali of *P. aguirrei* (Fig. 10a) are comparable in size, or even larger, than those of *M. merriami* (Harrison 1985), or the largest *Paracamelus* taxon known until now, *P. gigas* (Zdansky 1926 in Morales 1984). Even the smallest astragali of *P. aguirrei*, which is the astragalus studied by Morales (1984), is slightly larger than those of *P. alexejevi* (Havesson 1954 in Morales 1984) and all the *Camelus* species we have used for comparison in this paper (Martini et al. 2018; Martini and Geraads 2018), being ~5% wider. On the other hand, the largest astragalus of *P. aguirrei* is 13.5% wider than those from *P. alexejevi* and the *Camelus* species, 7% wider than *P. gigas*, and 3% wider than *Cp. hesternus* (Webb 1965).

The size of the calcaneus (Fig. 10b) in *P. aguirrei* is also comparable to that of *M. merriami* (Harrison 1985). The maximum height of *P. gigas* (Zdansky 1926 in Morales 1984; Teilhard and Trassaert 1937 in Titov and Logvynenko 2006) are somewhat smaller and those of *P.* cf. *aguirrei* (Titov and Logvynenko 2006) are also of the same height as the measurements of *P. aguirrei*. The calcaneus of all the other species compared in this study and even the first studied one of *P. aguirrei* (Morales 1984) are around between a 9% and a 6.5% smaller than the newly studied calcaneus of *P. aguirrei*.

The malleolar (Fig. 10c) of *P. aguirrei* shows a wide size variability, being similar in the same size to the extant species of *Camelus* (Martini et al. 2018) and *C. thomasi* (Martini and Geraads 2018).

As it happens with the malleolar (Fig. 10c), the cuboids (Fig. 10d) of *P. aguirrei* have from low-middle sizes to one of the largest measurements of all the sample, having a similar size than those of *C. bactrianus* (Martini et al. 2018) and *C. thomasi* (Martini and Geraads 2018).

The navicular of *P. aguirrei* (Fig. 10e) has one of the largest size values but is overpassed in its wide by the biggest forms of *C. bactrianus* (Martini et al. 2018) and *C. thomasi* (Martini and Geraads 2018) and in its height from the biggest forms of *C. bactrianus*, *C. thomasi* and *Cp. hesternus* (Webb 1965).

The proportions of the intermediolateral cuneiform of *P. aguirrei* (Fig. 10f) are a little bit larger than in the other taxa, being between a 10% and a 2.5% bigger in its maximum width and between 19% and 8% bigger in its lateral depth.

The phalanx size in *P. aguirrei* (Fig. 10g) has a big range of variations comparable in its minimum height to *P. alexejevi* (Havesson 1954 in Morales 1984), to one of the largest measurements, approaching the height of *M. merriami* (Harrison 1985). Also, they do not seem to follow the morpho-spatial trend of the extant species, which is more squared-like, but follow the trend of *M. merriami*, *C. thomasi* (Martini and Geraads 2018), and the rest of the *Paracamelus* species, which is more rectangular-like.

The most striking case is the metacarpal II-IV as there is a difference in correlations in the spatial trend when compared to other taxa. The figure of the epiphysis (Fig. 9e) shows that the proximal epiphysis of the metacarpal of *P. aguirrei* fall in the same diagonal as all the other camelid taxa, while in Fig. 9f the measurement (maximum length of the metacarpal by the maximum width of the proximal epiphysis) of *P. aguirrei* is located in the same diagonal than *M. merriami* (Harrison 1985), and *C. thomasi* (Martini and Geraads 2018), but not in the same space than the extant *Camelus* (Martini et al. 2018), *C. knoblochi* (Titov 2008, and references therein) or *Cp. hesternus* (Webb 1965). Also, the maximum length of *P. aguirrei* for the figure of the metacarpal (Fig. 9f) seems to be quite large in comparison with the width of the same element in the figure of the epiphysis (Fig. 9e). In addition, since there is an even larger *P. aguirrei* epiphysis lacking the diaphysis, the maximum length of the metacarpal of this species could be quite larger than thought.

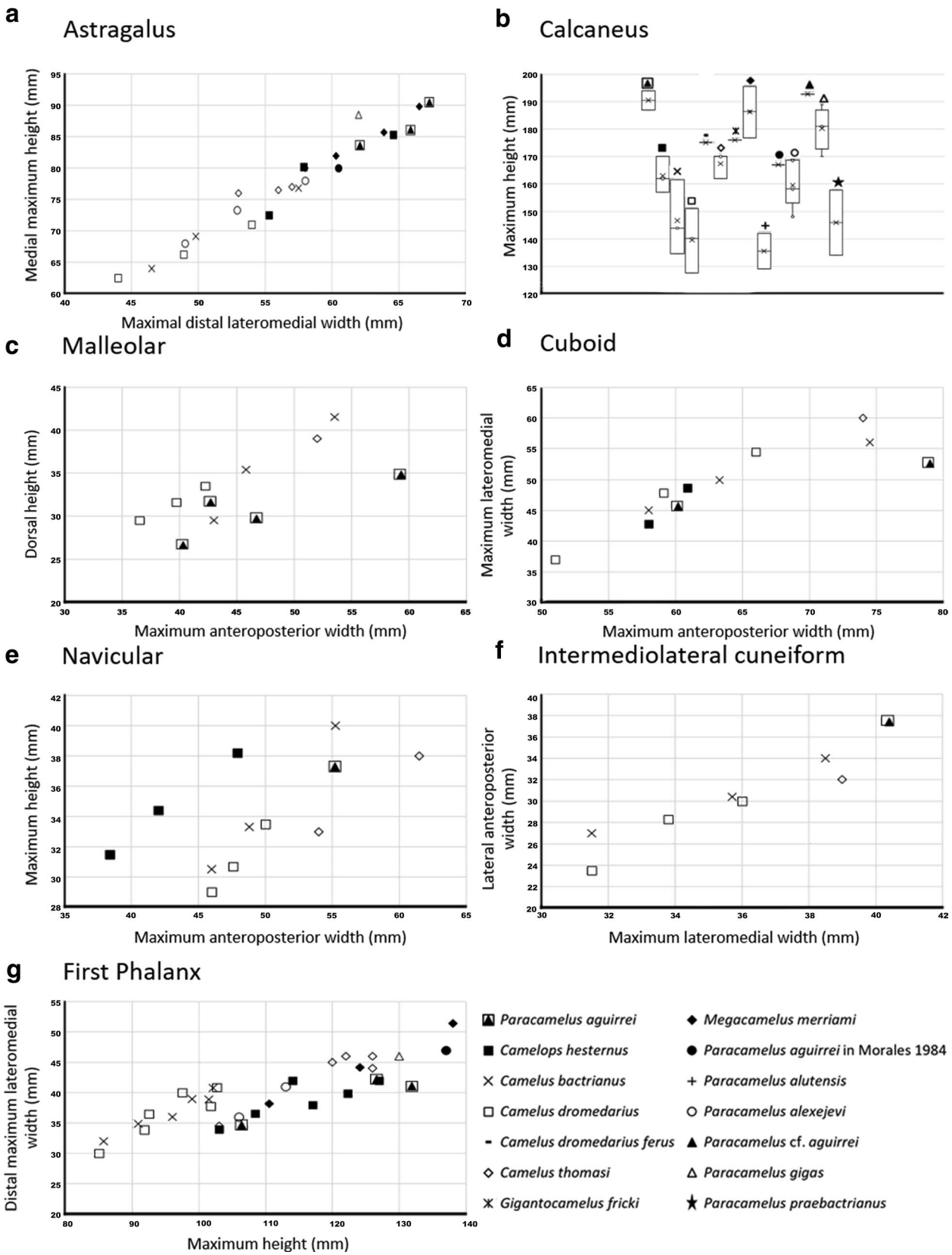

Fig. 10 Bivariate plots of the astragalus (**a**); calcaneus (**b**), malleolar (**c**), cuboid (**d**), navicular (**e**), intermediolateral cuneiform (**f**) and first phalanx (**g**)

5 Discussion and conclusions

The general dental and postcranial morphology of *P. aguirrei* is relatively close to that of other *Paracamelus* species, consequently species of this genus have been primarily differentiated by its size, as stated by Morales (1984). The description of the new camel autopodial bones from Venta del Moro allows us to perform a more accurate morphological comparison with other genera and species such as *C. dromedarius*, *Cp. hesternus* (Webb 1965; Zazula et al. 2016), *C. thomasi* (Martini and Geraads 2018), and *Titanotylopus* (Harrison 1979).

The metrical comparisons show that *P. aguirrei* is one of the largest derived camelids and one of the largest that ever existed. However, in the Venta del Moro sample, the smaller-size bones overlap with the homologous elements from other species. This size variability could be due to the presence of different individuals, so that some carpal bones may correspond to a relatively small specimen of *P. aguirrei*, while the tarsals would have belonged to a larger individual. In general, camels show an accused sexual dimorphism, which can be observed in the canines, pelvis, and overall size, being the males larger than the females (Martini et al. 2018). This sexual dimorphism would be especially marked in *P. aguirrei* of Venta del Moro. The size of the autopodial bones of the camel from Venta del Moro is among the largest of other camelid species. The comparison of these new remains with the astragalus (Fig. 10a) and the calcaneus (Fig. 10b) of the first studied remains of *P. aguirrei* (Morales, 1984) leads us to think that those first studied remains could represent a female individual. Finally, the observed difference between the morphology of the proximal epiphysis of the metacarpal (Fig. 9e) and its maximum estimated length (Fig. 9f) could represent that *P. aguirrei* was a very slender camel for its size with relatively longer and thinner legs than the extant *Camelus* species.

Paracamelus aguirrei continues to be one of the most notable species in the Spanish Miocene fossil record, and the new fossils described here, together with unpublished remains that will be described shortly in another paper, will help to clarify the phylogenetic relationships between *P. aguirrei* with the North American forms, place where this group originated.

Acknowledgements The fieldwork in Venta del Moro was supported, from 1995 to 2012, by the Conselleria de Cultura of the Valencian Government, and by the Conselleria d'Empresa, Universitat i Ciència (Generalitat Valenciana) [Project number GV06/304], with the permission of the Ministerio de Fomento and the Company ADIF, of the Spanish Government. Project supported by the Spanish Ministerio de Ciencia e Innovación PGC2018-094122-B-100 and CGL2016-76431-P (AEI/FEDER, UE), the Research Groups CSIC 64 1538, CAM-UCM 910607 and PVC-GIUV, and the Generalitat de Catalunya (CERCA Programme, and Beatriu de Pinós contract 2017 BP 00223 from AGAUR to J.A.). One author (VDC) is the beneficiary of a postdoctoral fellowship from the Argentinian Consejo Nacional de Investigaciones Científicas y Técnicas (CONICET). We thank the reviewers for their useful comments and the editors of the Journal of Iberian Geology for their work.

References

Aguirre, E., Robles, F., Thaler, L., López Martínez, N., Alberdi, M. T., & Fuentes, C. (1973). Venta del Moro, nueva fauna finimiocena de Moluscos y Vertebrados. *Estudios Geológicos, 29*, 569–578.

Agustí, J., Garcés, M., & Krijgsman, W. (2006). Evidence for African-Iberian exchanges during the Messinian in the Spanish mammalian record. *Palaeogeography, Palaeoclimatology, Palaeoecology, 238*(5), 5–14.

Alba, D. M., Montoya, P., Pina, M., Rook, L., Abella, J., Morales, J., & Delson, E. (2015). First record of *Mesopithecus* (Cercopithecidae, Colobinae) from the Miocene of the Iberian Peninsula. *Journal of Human Evolution, 88,* 1–14.

Alberdi, M., Morales, J., Moyà, S., & Sanchiz, B. (1981). Macrovertebrados (Reptilia y Mammalia) del yacimiento finimioceno de Librilla (Murcia). *Estudios Geológicos, 37*, 307–312.

Barbour, E. H., & Schultz, C. B. (1939). A new giant camel *Gigantocamelus fricki*, gen. et sp. nov. *Bulletin of the University of Nebraska State Museum, 2*(2), 17–27.

Casas-Gallego, M., Lassaletta, L., Barrón, E., Bruch, A. A., & Montoya, P. (2015). Vegetation and climate in the eastern Iberian Peninsula during the pre-evaporitic Messinian (late Miocene). Palynological data from the Upper Turolian of Venta del Moro (Spain). *Review of Paleobotany and Palynology, 215*, 85–99.

Colombero, S., Bonelli, E., Pavia, M., Repetto, G., & Carnevale, G. (2017). *Paracamelus* (Mammalia, Camelidae) remains from the late Messinian of Italy: insights into the last camels of western Europe. *Historical Biology, 29*(4), 509–518.

Crespo, V. D., Sevilla, P., Mansino, S., Montoya, P., & Ruiz-Sánchez, F. J. (2018). Bats from the classical site of Venta del Moro (late Miocene, Eastern Spain). *Historical Biology, 30*(3), 317–326.

García-Alix, A., Minwer-Barakat, R., Martín Suárez, E., Freudenthal, M., Aguire, J., & Kaya, F. (2016). Updating the Europe–Africa small mammal exchange during the late Messinian. *Journal of Biogeography, 43,* 1336–1348.

Gibert, L., Scott, G. R., Montoya, P., Ruiz-Sánchez, F. J., Morales, J., Luque, L., et al. (2013). Evidence for an African–Iberian mammal dispersal during the pre-evaporitic Messinian. *Geology, 41*(6), 691–694.

Harrington, C. R. (2011). Pleistocene vertebrates of the Yukon Territory. *Quaternary Science Reviews, 30*(17–18), 2341–2354.

Harrison, J. A. (1979). Revision of the Camelinae (Artiodactyla, Tylopoda) and description of the new genus *Alforjas*. *The University of Kansas Paleontological Contributions, 95*, 1–20.

Harrison, J. A. (1985). Giant Camels from the Cenozoic of North America. *Smithsonian contributions to paleobiology, 57*, 1–29.

Havesson, J. I. (1954). Tertiary camels of the Eastern Hemisphere (genus *Paracamelus*). *Proceedings of Paleontological Institute*, 67, 100–161.

Honey, J. G., Harrison, J. A., Prothero, D. R., & Stevens, M. S. (1998). Camelidae. In C. M. Janis, K. M. Scott & L. L. Jacobs (Eds.), *Evolution of Tertiary Mammals of North America. Volume I: Terrestrial Carnivores, Ungulates and Ungulatelike Mammals* (pp. 439–462). Cambridge: Cambridge University Press.

Ji, R., Cui, P., Ding, F., Geng, J., Gao, H., Zhang, H., Yu, J., Hu, S., & Meng, H. (2009). Monophyletic origin of domestic bactrian camel (*Camelus bactrianus*) and its evolutionary relationship with the extant wild camel (*Camelus bactrianus ferus*). *Animal Genetics*, 40 (4), 377–382.

Kostopoulos, D. S., & Sen, S. (1999). Late Pliocene (Villafranchian) mammals from Sarikol Tepe, Ankara, Turkey. *Mitteilungen der Bayerische Staatsammlung für Paläontologie und historische Geologie*, 39, 165–202.

Labarca, R., Pino, M., & Recabarren, O. (2013). Los Lamini (Cetartiodactyla: Camelidae) extintos del yacimiento de Pilauco (Norpatagonia chilena): aspectos taxonómicos y tafonómicos preliminares. *Estudios Geológicos, 69*(2), 255–269.

Likius, A., Brunet, M., Geraads, D., & Vignaud, P. (2003). Le plus vieux Camelidae (Mammalia, Artiodactyla) d'Afrique: limite Mio-Pliocène, Tchad. *Bulletin de la Société géologique de France, 174*(2), 187–193.

Logvinenko, V. N. (2000). Camels (Camelidae, Tylopoda) of the Pliocene and Eopleistocene of Ukraine. *Vestnik zoologii*, Kiev, suppl, 14, 120–127.

Logvynenko, V. M. (2001). *Paracamelus minor* (Camelidae, Tylopoda): A new camelid species from the Middle Pliocene of Ukraine. *Vestaik zoologii, 35*(1), 39–42.

van der Made, J., & Morales, J. (1999). Family Camelidae. In G. E. Rössner & K. Heissig (Eds.), *The Miocene Land Mammals of Europe* (pp. 221–224). München: Verlag Dr. Friedrich Pfeil.

van der Made, J., Morales, J., & Montoya, P. (2006). Late Miocene turnover in the Spanish mammal record in relation to palaeoclimate and the Messinian Salinity Crisis. *Palaeogeography, Palaeoclimatology, Palaeoecology, 238*, 228–246.

van der Made, J., Morales, J., Sen, S., & Aslan, F. (2002). The first camel from the Upper Miocene of Turkey and the dispersal of the camels into the Old World. *Comptes Rendus Palevol, 1*, 117–122.

Mansino, S., Crespo, V. D., Montoya, P., & Ruiz-Sánchez, F. J. (2017). Muridae from the late Miocene site of Venta del Moro (Eastern Spain). *Historical Biology, 29*(5), 677–691.

Mansino, S., García-Alix, A., Ruiz-Sánchez, F. J., & Montoya, P. (2015). A new *Eliomys* from the Late Miocene of Spain, and its implications for the phylogeny of the genus. *Acta Paleontologica Polonia, 60*(3), 577–588.

Mansino, S., Ruiz-Sánchez, F. J., & Montoya, P. (2018). Sciuridae (Rodentia, Mammalia) from the Late Miocene of Venta del Moro (Cabriel Basin, Spain): biostratigraphical, phylogenetic and palaeoecological inferences. *Historical Biology, 30*(3), 297–304.

Mansino, S., Ruiz-Sánchez, F. J., Freudenthal, M., & Montoya, P. (2014). A new approach to the Late Miocene-Early Pliocene forms of the genus *Apocricetus*. *Apocricetus alberti* (Rodentia, Mammalia) from Venta del Moro (Cabril Basin, Spain). *Proceedings of the Geologists' Association, 125*, 392–405.

Martini, P., & Geraads, D. (2018). *Camelus thomasi* Pomel, 1893 from the Pleistocene type-locality Tighennif (Algeria). Comparisons with modern *Camelus*. *Geodiversitas, 40*(5), 115–134.

Martini, P., Schmid, P., & Costeur, L. (2018). Comparative morphometry of bactrian camel and dromedary. *Journal of Mammalian Evolution, 25,* 407–425.

Mein, P. (1975). Proposition de Biozonation du Néogène Méditerranéen à partir des Mammifères. *Trabajos sobre Neógeno-Cuaternario, 4*, 112–113.

Montoya, P., Morales, J., & Abella, J. (2009). *Eucyon debonisi* n. sp., a new Canidae (Mammalia, Carnivora) from the latest Miocene of Venta del Moro (Valencia, Spain). *Geodiversitas, 31*(4), 709–722.

Montoya, P., Morales, J., & Abella, J. (2011). Musteloidea (Carnivora, Mammalia) from the Late Miocene of Venta del Moro (Valencia, Spain). *Estudios Geológicos, 67*(2), 193–206.

Montoya, P., Morales, J., Robles, F., Abella, J., Benavent, J. V., Marín, M. D., & Ruiz-Sánchez, F. J. (2006). Las nuevas excavaciones (1995–2006) en el yacimiento del Mioceno final de Venta del Moro. *Valencia. Estudios Geológicos, 62*(1), 313–326.

Morales, J. (1984). *Venta del Moro: su macrofauna de mamíferos y bioestratigrafía continental de Mioceno terminal mediterráneo*. PhD. Thesis. Universidad Complutense de Madrid, 340 p.

Morales, J., & Aguirre, E. (1976). Carnívoros de Venta del Moro. *Trabajos sobre Neógeno-Cuaternario, 5*, 31–74.

Morales, J., Montoya, P., & Abella, J. (2011). Venta del Moro: un yacimiento clave para conocer la historia del límite Mio-Plioceno en el área mediterránea. *Isurus, 4*, 60–71.

Morales, J., Peláez-Campomanes, P., Abella, J., Montoya, P., Ruiz, F. J., Gibert, L., Scott, G., Cantalapiedra, J. L., & Sanisidro, O. (2013). The Ventian mammal age (Latest Miocene): present state. [La edad de mamíferos ventienses (Mioceno terminal): estado actual]. *Spanish Journal of Palaeontology, 28*(2), 149–160.

Morales, J., Soria, D., & Aguirre, E. (1980). Camélido Finimioceno en Venta del Moro. Primera cita para Europa occidental. *Estudios Geológicos, 36*, 139–142.

Mukasa-Mugerwa, E. (1981). *The camel (Camelus dromedarius): a bibliographical review*. Addis Ababa: International livestock Centre for Africa.

Orlov, Y. A. (1929). Ueber die Reste der fossilen Cameliden aus dem Gouv, Akmolinsk (Westsiberien). *Annuaire du Musee Zoologique de l'Académie Des Sciences de l'USSR, 30*, 549–587.

Pérez-Lorente, F., Herrero, C., Herrero, E., Montoya, P., & Murcia. (2009). *Paracamelichnum jumillensis* n.ichnogen. n.ichonsp., Upper Miocene Camelidae Ichnites from the Hoya de la Sima site, Spain. *Ichnos, 16,* 208–219.

Pesquero, M. D., Alberdi, M. T., & Montoya, P. (2007). *Hipparion* (Equidae, Mammalia) from Venta del Moro (Valencia Province, Spain). *Neues Jahrbuch für Geologie und Paläontologie - Abdhanlungen, 243*, 273–297.

Pickford, M., Morales, J., & Soria, D. (1993). First fossil camels from Europe. *Nature, 365*(6448), 701.

Pickford, M., Morales, J., & Soria, D. (1995). Fossil camels from the Upper Miocene of Europe: Implications for biogeography and faunal change. *Geobios, 28*(5), 641–650.

Prothero, D. R., & Schoch, R. M. (2002). *Horns, Tusks, and Flippers: The evolution of hoofed mammals*. Baltimore: The Johns Hopkins University Press.

Rybczynski, N., Gosse, J. C., Harington, C. R., Wogelius, R. A., Hidy, A. J., & Buckley, M. (2013). Mid-Pliocene warm-period deposits in the High Arctic yield insight into camel evolution. *Nature Communications*. https://doi.org/10.1038/ncomms2516

Salesa, M. J., Antón, M., Turner, A., Alcalá, L., Montoya, P., & Morales, J. (2010). Systematic revision of the Late Miocene sabretoothed felid *Paramachaerodus* in Spain. *Palaeontology, 53*(6), 1369–1391.

Schlosser, M. (1903). Die fossilen Saugetiere Chinas nebst einer Odontographie der rezenten Antilopens. *Abhandlungen der Königlichen bayertschen Akademte der Wissenschaften, Mathematisch-naturwissen-schaftliche Klasse, 12*, 1–221.

Teilhard, P., & Trassaert, M. (1937). The Pliocene Camelidae, Giraffidae and Cervidae of South Eastern Shauai. *Paleontologia Sinica, 102*, 1–69.

Titov, V. V. (2008). Habitat conditions for *Camelus knoblochi* and factors in its extinction. *Quaternary International, 179,* 120–125.

Titov, V. V., & Logvynenko, V. N. (2006). Early *Paracamelus* (Mammalia, Tylopoda) in Eastern Europe. *Acta Zoologica Cracoviensia, 49A*(1–2), 163–178.

Wang, X., Flynn, L. J., & Fortelius, M. (2013). *Mammals of Asia. Neogene Biostratigraphy and Chronology*. New York: Columbia University Press.

Webb, S. D. (1965). The Osteology of *Camelops*. *Bulletin of the Los Angeles County Museum, Science, 1*, 1–54.

Zazula, G. D., Macphee, R. D. E., Hall, E., & Hewitson, S. (2016). Osteological assessment of Pleistocene *Camelops hesternus* (Camelidae: Camelinae: Camelini) from Alaska and Yukon. *American Museum Novitates, 3866*, 1–45.

Zdansky, O. (1926). *Paracamelus gigas* Schlosser. *Paleontologia Sinica, 2*(C;4), 1–44.